



# Modeling larval recruitment dynamics of eastern oysters *Crassostrea virginica* with implications for restoration and management of oyster fisheries

Chengxue Li<sup>1,2,\*</sup>, Hui Liu<sup>1</sup>

<sup>1</sup>Department of Marine Biology, Texas A&M University at Galveston, Galveston, Texas 77553, USA

<sup>2</sup>Present address: NOAA Northeast Fisheries Science Center, Woods Hole, Massachusetts 02543, USA

**ABSTRACT:** Increasing attention has been devoted to understanding the responses of oyster populations to natural disasters such as hurricanes. In particular, the recruitment of planktonic oyster larvae is crucial to the recovery and sustainability of oyster populations and, by extension, oyster fisheries. In this study, a bioenergetic model was developed to explore the spatio-temporal dynamics of larval recruitment for the eastern oyster *Crassostrea virginica* within the Galveston Bay System of Texas, USA. Further, model simulations were performed for a case study under post-hurricane (2018) and normal (2021) scenarios, aiming to elucidate the response mechanisms of oyster larvae to the hurricane disturbance. Our results demonstrate a strong post-hurricane recovery of planktonic oysters in 2018. Simulated larval recruitment was much higher in the middle–lower Galveston Bay and West Bay compared to the upper Galveston Bay and East Bay. By using simulation results, we further quantified the planktonic habitat suitability for oyster larvae to support future oyster management and restoration. This study contributes to the quantitative assessment of oyster resilience and adaptation in the face of the escalating threat of hurricanes amidst climate change and provides a framework for future coupling of an individual-based model with a biophysical model to enhance understanding of oyster larval dispersal and population connectivity.

**KEY WORDS:** *Crassostrea virginica* · Larvae · Recruitment dynamics · Restoration · Hurricanes · Climate change

## 1. INTRODUCTION

The eastern oyster *Crassostrea virginica* is not only a commercially important species but also provides essential habitats for other marine organisms, along with numerous ecological services (Coen et al. 2007, Grabowski et al. 2012). However, due to climate and human perturbations, oyster reefs have experienced a nearly 85% decline globally (Jackson 2001, Beck et al. 2011). To address this ongoing habitat loss, much attention has been focused on oyster restoration and management.

In the northern Gulf of Mexico (nGoM), oyster reef depletion has been exacerbated by natural disasters such as hurricanes (Buck 2005, Tunnell 2017, Martinez et al. 2022). For example, hurricane-driven wave dam-

age and sediment deposits can directly cause massive oyster die-offs (Du et al. 2021). While post-hurricane rainfall and freshwater discharge may further reduce oyster survival (Buzan et al. 2009, Pollack et al. 2011, Park et al. 2014), nutrient enrichment, reduced predation pressure, and lower disease prevalence following the hurricane may enhance oyster recovery (Livingston et al. 1999). Therefore, understanding the response of oysters after hurricanes is of scientific interest for supporting strategic conservation, restoration, and management of oyster fisheries.

Hurricane Harvey in August 2017 greatly disturbed the Galveston Bay System (GBS), a major oyster harvesting area in Texas, USA, with record-breaking rainfall (Du & Park 2019). The resultant floods displaced about 3 times the volume of the GBS, making

\*Corresponding author: [chengxue.li@noaa.gov](mailto:chengxue.li@noaa.gov)

the bay a freshwater system for several days (Du & Park 2019). This extreme weather event and the associated impacts on the GBS provide an ideal scenario to examine oyster resilience following hurricanes.

The resilience of oysters can be directly linked to the recruitment of their planktonic larvae (Park et al. 2014), but establishing this connection is challenging in practice due to limited field observations and difficulties in species identification. To bridge this knowledge gap, the present study focuses on the pelagic life stages of oysters and combines observations with modeling techniques to understand how oyster larvae are influenced by hurricane disturbance.

The planktonic larval duration (PLD) for oysters is typically less than 30 d (Deksheniaks et al. 1993). During this period, recruitment to benthic settlement habitats is an integrated result of biological and physical processes (Narváez et al. 2012). While many studies have applied biophysical models to examine dynamics of oyster larvae over space and time (North et al. 2008, Kim et al. 2013), these models primarily focused on physical aspects, with less attention paid to the integration of physiology with physical processes of planktonic larvae.

Modeling population dynamics should be guided by species biology with careful considerations of the relationships between biological processes and time-varying environmental conditions (Bi & Liu 2017, Li & Liu 2022). In the present study, our aim was to develop an individual-based model for eastern oyster larvae built upon a framework of the dynamic energy budget model (DEBM) (Kooijman 2000). The DEBM tracks the processes of energy flow of an organism from food intake to growth, development, metabolism, and reproduction, with environmental factors included as rate-controlling factors. We applied the DEBM, with incorporation of *in situ* observations, to simulate the spatio-temporal dynamics of oyster larvae in the GBS both in 'post-hurricane' (2018) and 'normal' (2021) scenarios during the oyster spawning season (May–July). The study design for side-by-side comparisons aids in better understanding the mechanisms of oyster recruitment in response to hurricane disturbance.

Evaluating habitat suitability is crucial for oyster restoration (Beseres Pollack et al. 2012, Soniat et al. 2013). However, little attention has been paid to quantifying habitat suitability for oysters during their planktonic phase. Here, for the first time, we synthesize 3 biologically meaningful indices (larval production, survival, and growth) to introduce and evaluate planktonic habitat suitability for oyster larvae. Our findings support future oyster management strategies, such as establishing sanctuaries as sources of

larval supplies to enhance aquaculture, conservation, and restoration efforts.

## 2. MATERIALS AND METHODS

### 2.1. Study area

The GBS, comprising Trinity Bay, Galveston Bay, East Bay, and West Bay (Fig. 1A), is one of the largest estuaries along the nGoM coast and serves as the dominant commercial oyster harvesting area in Texas (Buzan et al. 2009). Freshwater inflow into the GBS is mainly contributed by the Trinity River (55%), San Jacinto River (16%), and Buffalo Bayou (12%) (Guthrie et al. 2012). The GBS is a shallow micro-tidal estuary, with an average depth of approximately 2 m and a tidal range of less than 0.5 m. The Lagrangian residence time varies from 15 d (ship channel) to 45 d (upper bay) depending upon the location and time (Rayson et al. 2016). The hydrology of the GBS results in a wide range of salinity regime from the upper bay to the lower bay, with an average of 16 (Orlando et al. 1993). Additionally, the bay has low to moderate chlorophyll *a* (chl *a*) concentrations, ranging from 2 to 45  $\mu\text{g l}^{-1}$  (Roelke et al. 2013).

### 2.2. Data acquisition

Oyster larvae were sampled at 5 long-term zooplankton monitoring stations in the GBS (Fig. 1A; Liu et al. 2017, 2021) during May, June, and July of 2018 and 2021. Additional stations were visited in 2021 to expand the spatial coverage of our study area (Fig. 1A). Details of the sampling dates, locations, and number of samples are provided in Table S1 in the Supplement at [www.int-res.com/articles/suppl/m756p031\\_supp.pdf](http://www.int-res.com/articles/suppl/m756p031_supp.pdf). Zooplankton sampling was conducted using horizontal net tows in the upper water column (depth <1.5 m). Two plankton nets (mesh size: 100 and 200  $\mu\text{m}$ ; dimensions: 30 cm diameter, 120 cm in length) were deployed and towed simultaneously with a speed of 1.5–2.0 knots for at least 5 min. Digital flowmeters were mounted in the center of the net mouth to record the volume of seawater filtered. Upon retrieval onto the deck, zooplankton samples were transferred into a 500 ml jar with 10% buffered formalin and seawater solution.

Zooplankton collected from the 100  $\mu\text{m}$  net were processed in the laboratory following the protocols outlined by Liu et al. (2021). Planktonic oyster larvae from each sample were enumerated and classified into



5 stages: 74, 138, 240, 276, and 330  $\mu\text{m}$ , based on their size and morphology (see Fig. 1 in Deksheniaks et al. 1993). Subsamples composed of at least  $\sim 10\%$  of the total sample were processed. The density of oyster larvae was calculated by dividing the number of oyster larvae from one sample by the total volume of water filtered.

Surface water temperature and salinity data were obtained from the Northern Gulf of Mexico Operational Forecast System (<https://www.ncei.noaa.gov/data/>), based on simulations from the Finite Volume Coastal Ocean Model (FVCOM) (Yang et al. 2016). The FVCOM simulation was generated every 6 h, and the daily average was calculated. Validation of the FVCOM simulations was performed using observed data collected from 3 monitoring stations (<https://waterdatafortexas.org/coastal>). Details of the validation results are provided in Fig. S1.

Daily near-surface chl  $a$  concentrations, with a spatial resolution of 750 m, were derived from the Visible Infrared Imaging Radiometer Suite on the Suomi National Polar-orbiting Partnership satellite (<https://coastwatch.noaa.gov/erddap/griddap/>). Validation of the satellite data was conducted using field-observed chl  $a$  concentrations at 5 stations from May to July 2018 (Liu et al. 2021). Details of the validation results can be found in Fig. S2.

The conversion equation from chl  $a$  concentration ( $\mu\text{g l}^{-1}$ ) to phytoplankton biovolume ( $X$ ,  $\mu\text{m}^3 \mu\text{l}^{-1}$ ) was adopted from a study conducted in adjacent coastal waters (Schaeffer et al. 2012):

$$X = 165.23 \times (\text{Chl } a)^{1.2504} \quad R^2 = 0.65 \quad (1)$$

The model domain in this study fully covers the oyster reefs in the GBS, with a spatial resolution of  $0.02^\circ$  latitude/longitude (Fig. 1B). Missing data were filled in using inverse distance weighted interpola-

tion with a power of 2. Daily surface water temperature and salinity from the hydrodynamic model were aggregated to match the spatial resolution of the model domain. Daily chl  $a$  data were aggregated to provide monthly values. Additionally, water depth data collected from Texas Parks and Wildlife Department (TPWD) surveys were interpolated to the model grid cells.

### 2.3. Model description

In the DEBM, the energy uptake is assimilated and stored in an energy reserve ( $E$ ), which is allocated to 3 sectors: (1) somatic growth, (2) maintenance, and (3) maturity and reproduction (Kooijman 2000). For larval stages, energy used for maturity and reproduction is directly re-allocated to development (e.g. increase in body complexity) (Kooijman 2000, Pouvreau et al. 2006). As illustrated in Fig. 2, the energy in the reserve pool ( $E$ ) is allocated to support somatic growth ( $P_G$ ), growth-related maintenance ( $P_{M1}$ ), development ( $P_D$ ), and development-related maintenance ( $P_{M2}$ ).

While most species-specific parameters of eastern oyster larvae were gleaned from empirical studies, some were borrowed from their sibling species (Table 1). Notations and symbols used in the current DEBM are largely consistent with Kooijman (2000) and are described as follows: square brackets, [ ], and braces, { }, represent quantities per unit of structural biovolume and biosurface, respectively. Dots above letters are referred to as rates (i.e. change over time).

In the DEBM, an individual oyster larva absorbs energy through the ingestion of phytoplankton in the water column. The assumption is that the gross energy ingested by an individual is proportional to

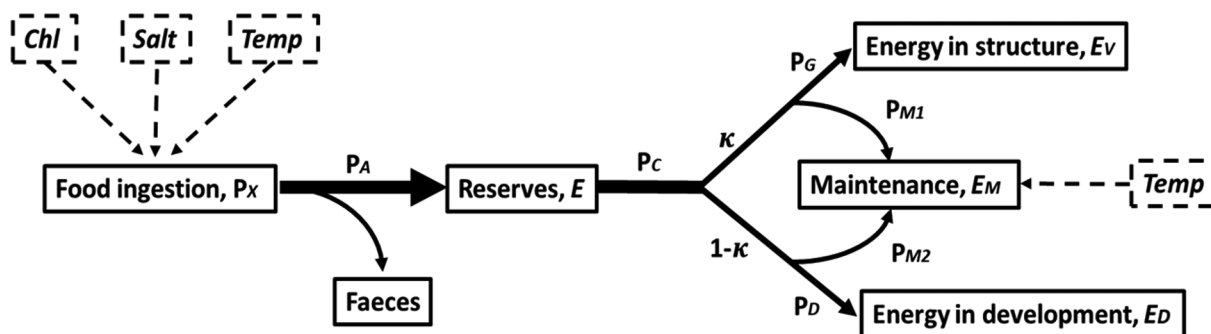


Fig. 2. Dynamic energy budget model (DEBM) for eastern oyster larvae. Chlorophyll  $a$  (chl  $a$ ) concentration ( $\mu\text{g l}^{-1}$ ), temperature ( $^\circ\text{C}$ ), and salinity are the 3 main drivers controlling the bioenergetics of oyster larvae. In the DEBM, the energy uptake is assimilated and stored as energy reserves ( $E$ ). A proportion  $\kappa$  of the assimilated energy is used for somatic growth ( $P_G$ ) and growth-related maintenance ( $P_{M1}$ ), and a proportion  $1 - \kappa$  of the assimilated energy is used for development ( $P_D$ ) and development-related maintenance ( $P_{M2}$ )

Table 1. Parameters in the dynamic energy budget model (DEBM) for eastern oyster larvae. Notations and symbols used in the current DEBM are largely consistent with Kooijman (2000) and are described as follows: square brackets, [ ], and braces, { }, represent quantities per unit of structural biovolume and biosurface, respectively

Parameter definition	Symbol	Value	Unit	Source
<b>Key parameters</b>				
Maximum surface-specific ingestion rate	$\{\dot{P}_{Xm}\}$	$6.165 \times 10^{-7}$	$\text{J d}^{-1} \mu\text{m}^{-2}$	Rico-Villa et al. (2010) <sup>a</sup>
Maximum surface-specific clearance rate	$C_R$	137	$\mu\text{m}^3 \text{d}^{-1} \mu\text{m}^{-2}$	Rico-Villa et al. (2010) <sup>a</sup>
Energy content of phytoplankton biovolume	$\mu_X$	$4.5 \times 10^{-9}$	$\text{J} \mu\text{m}^{-3}$	Rico-Villa et al. (2010) <sup>a</sup>
Half saturation coefficient	$K$	600	$\mu\text{m}^3 \mu\text{l}^{-1}$	Rico-Villa et al. (2010) <sup>a</sup>
Assimilation efficiency	$\kappa_X$	0.4	—	Sprung (1984) <sup>b</sup>
Volume-specific maintenance rate	$[P_M]$	24	$\text{J} \mu\text{m}^{-3}$	Pouvreau et al. (2006) <sup>a</sup>
Maximum surface-specific assimilation rate	$\{\dot{P}_{Am}\}$	$2.466 \times 10^{-7}$	$\text{J d}^{-1} \mu\text{m}^{-2}$	Pouvreau et al. (2006) <sup>a</sup>
Energy density capacity	$[E_M]$	$2.295 \times 10^{-9}$	$\text{J} \mu\text{m}^{-3}$	Pouvreau et al. (2006) <sup>a</sup>
Volume-specific energy expenditure for somatic growth	$[E_G]$	$1.9 \times 10^{-9}$	$\text{J} \mu\text{m}^{-3}$	Pouvreau et al. (2006) <sup>a</sup>
Energy conductance	$\dot{v}$	107.451	$\mu\text{m d}^{-1}$	Rico-Villa et al. (2010) <sup>a</sup>
Allocation fraction to somatic growth and its maintenance	$\kappa$	0.45	—	Rico-Villa et al. (2010) <sup>a</sup>
Shape coefficient	$\delta_M$	0.658	—	Rico-Villa et al. (2010) <sup>a</sup>
<b>Temperature effect</b>				
Arrhenius temperature	$T_A$	6700	K	Lavaud et al. (2017) <sup>c</sup>
Reference temperature	$T_1$	293	K	Lavaud et al. (2017) <sup>c</sup>
Lower boundary of the tolerance range	$T_L$	283	K	Galtsoff (1964) <sup>c</sup>
Upper boundary of the tolerance range	$T_H$	303	K	Galtsoff (1964) <sup>c</sup>
Arrhenius temperature for lower boundary	$T_{AL}$	21820	K	Lavaud et al. (2017) <sup>c</sup>
Arrhenius temperature for upper boundary	$T_{AH}$	45380	K	Lavaud et al. (2017) <sup>c</sup>
<b>Salinity effect</b>				
Lower limit of salinity tolerance	$S_L$	7.5	psu	Davis (1958) <sup>c</sup>
Upper limit of salinity tolerance	$S_H$	15	psu	Davis (1958) <sup>c</sup>
<sup>a</sup> Parameters of the Pacific oyster <i>Crassostrea gigas</i>				
<sup>b</sup> Parameters of the blue mussel <i>Mytilus edulis</i>				
<sup>c</sup> Parameters of the eastern oyster <i>Crassostrea virginica</i>				

the biosurface (or squared length) of an organism. The ingestion rate of an individual, which varies depending on environmental conditions, can be expressed as follows:

$$\dot{P}_X = \{\dot{P}_{Xm}\} \cdot f \cdot V^{2/3} \cdot \alpha_T \cdot \alpha_S \quad (2)$$

where  $\dot{P}_X$  is the ingestion rate ( $\text{J d}^{-1}$ ) and  $V$  is the volume of the animal body ( $\mu\text{m}^3$ ). Coefficients  $\alpha_T$  and  $\alpha_S$  represent the effect of water temperature and salinity on species ingestion, respectively.  $\{\dot{P}_{Xm}\}$  is the maximum surface-specific ingestion rate ( $\text{J d}^{-1} \mu\text{m}^{-2}$ ), which is calculated by:

$$\{\dot{P}_{Xm}\} = C_R \cdot \mu_X \quad (3)$$

where  $C_R$  is the maximum surface-specific clearance rate ( $\mu\text{m}^3 \text{d}^{-1} \mu\text{m}^{-2}$ ), and  $\mu_X$  is the estimated energy content of microalgae ( $\text{J} \mu\text{m}^{-3}$ ).

The scaled functional response for feeding ( $f$ ), ranging from 0 to 1, is assumed to follow a type III Holling's (1959) equation according to Rico-Villa et al. (2010):

$$f = \frac{X^2}{X^2 + K^2} \quad (4)$$

where  $K$  is the half saturation coefficient ( $\mu\text{m}^3 \mu\text{l}^{-1}$ ), and  $X$  is the chl  $a$  concentration from Eq. (1).

The assimilation rate of an oyster larva,  $\dot{P}_A$  ( $\text{J d}^{-1}$ ), is given as:

$$\dot{P}_A = \kappa_X \cdot \dot{P}_X = \{\dot{P}_{Am}\} \cdot f \cdot V^{2/3} \cdot \alpha_T \cdot \alpha_S \quad (5)$$

where  $\kappa_X$  is the assimilation coefficient, and  $\{\dot{P}_{Am}\}$  is the maximum surface-specific assimilation rate expressed in  $\text{J d}^{-1} \mu\text{m}^{-2}$ .

The dynamics of energy reserve ( $E$ ) is the difference between energy input from food assimilation ( $\dot{P}_A$ ) and the energy consumption ( $\dot{P}_C$ ) that fuels all metabolic processes:

$$\frac{dE}{dt} = \dot{P}_A - \dot{P}_C \quad (6)$$

According to Kooijman (2000), the temperature-dependent catabolic rate is governed by:

$$\dot{P}_C = \frac{\sigma_T \cdot [E] \cdot ([E_G] \cdot \dot{v} \cdot V^{2/3} + [P_M])}{\kappa \cdot [E] + [E_G]} \quad (7)$$

where  $[E] = E/V$  is the reserve density ( $J \mu m^{-3}$ );  $\dot{v} = \{\dot{P}_{Am}\}/[E_M]$  is the energy conductance ( $\mu m d^{-1}$ ), with  $[E_M]$  being the energy density capacity ( $J \mu m^{-2}$ );  $[\dot{P}_M]$  is the volume-specific maintenance rate ( $J d^{-1} \mu m^{-3}$ );  $[E_G]$  is the volume-specific cost for somatic growth; and  $\kappa$  is a fixed allocation fraction of mobilized reserve flux for somatic growth and growth-related maintenance.

Based on the 'κ-rule' of Kooijman (2000), the allocation rate of somatic growth ( $\dot{P}_G$ ,  $J d^{-1}$ ) is the rest of a proportion  $\kappa$  of mobilized reserve after deducting growth-related maintenance ( $\dot{P}_{M1}$ ,  $J d^{-1}$ ):

$$\frac{dE_G}{dt} = \dot{P}_G = \kappa \cdot \dot{P}_C - \dot{P}_{M1} \quad (8)$$

where  $\dot{P}_{M1} = [\dot{P}_M] \cdot V$ , with  $[\dot{P}_M]$  being the volume-specific somatic maintenance rate. Note that energy used for growth-related maintenance has priority over that for structural growth. That is, when needed, the energy subdivided into somatic growth can be revoked to compensate for growth-related maintenance.

The change in structural volume per unit time can be calculated by:

$$\frac{dV}{dt} = \frac{\dot{P}_G}{[E_G]} \quad (9)$$

In the DEBM, physical length ( $L_\omega$ ) is scaled to volumetric length ( $L$ ) by multiplying a shape coefficient ( $\delta_M$ ):  $L = \delta_M L_\omega$ . The change in physical length is formulated according to Monaco et al. (2014):

$$\frac{dL_\omega}{dt} = \left( \frac{\dot{P}_G}{[E_G]} \right) / \frac{1}{3L^2 \delta_M} \quad (10)$$

A proportion of  $1 - \kappa$  of energy is allocated to support development ( $\dot{P}_D$ ,  $J d^{-1}$ ) and its maintenance ( $\dot{P}_{M2}$ ,  $J d^{-1}$ ). An equation to calculate the remaining fraction for development is:

$$\frac{dE_D}{dt} = \dot{P}_D = (1 - \kappa) \cdot \dot{P}_C - \dot{P}_{M2} \quad (11)$$

where  $\dot{P}_{M2} = [\dot{P}_M] \cdot V \cdot (1 - \kappa) / \kappa$ . Again, the energy needed for development is always secondary after development maintenance.

Ingestion and maintenance are temperature dependent. The present study applies a temperature correction factor for physiological rates based on the Arrhenius relationship (Lavaud et al. 2017):

$$\alpha_T = \exp \left\{ \frac{T_A}{T_1} - \frac{T_A}{T} \right\} \cdot \frac{1 + \exp \left\{ \frac{T_{AL}}{T_1} - \frac{T_{AL}}{T_L} \right\} + \exp \left\{ \frac{T_{AH}}{T_H} - \frac{T_{AH}}{T_L} \right\}}{1 + \exp \left\{ \frac{T_{AL}}{T} - \frac{T_{AL}}{T_L} \right\} + \exp \left\{ \frac{T_{AH}}{T_H} - \frac{T_{AH}}{T} \right\}} \quad (12)$$

where  $T_A$  is the Arrhenius temperature (K),  $T_1$  is the reference temperature (K),  $T_{AH}$  and  $T_{AL}$  are the Arrhenius temperature for the rate of decrease at upper and lower boundaries (K),  $T_L$  and  $T_H$  are the lower and upper boundaries of the tolerance range (K). The assumption is that within the tolerance range, the physiological rate increases/decreases exponentially as temperature increases/decreases, while outside the optimal range, the physiological rate reduces at both low and high temperatures (van der Veer et al. 2006).

The salinity effect on ingestion is given below (Lavaud et al. 2017):

$$\alpha_S = \begin{cases} 0 & \text{when } S \leq S_L \\ \frac{S - S_L}{S_H - S_L} & \text{when } S \in (S_L, S_H) \\ 1 & \text{when } S \geq S_H \end{cases} \quad (13)$$

## 2.4. Model assumptions

Oyster larvae tend to reduce or even cease their growth and development in unfavorable conditions. However, in some extreme conditions when energy investment to the 'κ' branch of assimilation cannot meet the somatic maintenance requirement (i.e.  $\kappa \cdot \dot{P}_C < \dot{P}_{M1}$ ), oyster larvae are assumed to enter 'starvation' mode. Specifically, the energy deficit is directly paid from the '1 - κ' branch of assimilation, and all development-related processes are completely suspended (Jager & Ravagnan 2015). When the reserve mobilization is still not sufficient to meet the maintenance demand, starvation-induced body shrinkage is assumed to be initiated for survival (Pouvreau et al. 2006). This shrinkage during starvation is reversible once the condition recovers. The shrinkage rate with respect to structural volume is given as:

$$\frac{dV}{dt} = \frac{\dot{P}_{M1} - \dot{P}_C}{[E_G]} \quad (14)$$

PLD varies across seasons and geographic locations, ranging from 10 to 30 d (Dekshenieks et al. 1993, Powell et al. 1995, Kennedy 1996, Narváez et al. 2012). Hence, in the DEBM, each planktonic larva with delayed growth is forced to die when its PLD exceeds the maximum pelagic span of 30 d.

Sources of larval oyster mortality consist of starvation mortality ( $M_S$ ) and natural mortality ( $M_n$ ). In the DEBM, starvation mortality occurs when the energy reserve ( $E$ ) is  $\leq 0$  or when the body size shrinks to  $50 \mu m$ . Natural mortality is assumed to be  $20\% d^{-1}$  (Quayle 1964) and remains constant across stages.

From the above, oyster larval abundance at the next time step  $N_{(t+1)}$  can be described as:

$$N_{(t+1)} = N_{(t)} - N_{M_s(t)} - N_{M_n(t)} \quad (15)$$

where  $N_{(t)}$ ,  $N_{M_s(t)}$ , and  $N_{M_n(t)}$  denote oyster larval abundance, starvation mortality, and natural mortality at time  $t$ , respectively. The time step in the model is 1 d.

Substantial mortality of pre-settling oyster larvae that reach a size of 330  $\mu\text{m}$  can occur during their metamorphosis and settlement (Haws et al. 1993, Klein et al. 2023). We assumed the daily settlement rate to be 20% for the pre-settling larvae (Jones & Jones 1983). The energy demand for metamorphosis varies between 5.4 and 7.7  $\text{mJ ind.}^{-1}$  (García-Esquivel et al. 2001). Our preliminary results showed that most (>95%) pre-settling larvae in Galveston Bay had energy reserves over 5.4  $\text{mJ}$ . For simplicity, metamorphic success is not modeled here. In the model, the settled larvae are ideally assumed to instantly become spat and disappear from the planktonic cohorts (Rico-Villa et al. 2010).

Individual variations in life-history traits play an important role in shaping oyster populations (Smee et al. 2013, Hanley et al. 2016). In the present study, stages 1–5 refer to planktonic stages and stage 6 refers to the spat stage. The initial sizes of planktonic oyster larvae from stage 1 to 5 are assumed to follow a normal distribution with means of 74, 138, 240, 276, and 330  $\mu\text{m}$ , respectively, with no individuals assumed to have reached stage 6. To represent individual variability in natural oyster larvae, the initial size was randomly selected from a normal distribution with mean ( $\mu$ ) and standard deviation ( $\text{SD} = 10\% \times \mu$ ) representing the corresponding size class (Bi & Liu 2017, Li & Liu 2022). In addition, a general coefficient of variation (CV) of 10% ( $\text{SD} = 10\% \times \mu$ ) is assigned to the half-saturation coefficient ( $K$ ) and shape coefficient ( $\delta_M$ ). The range of these parameters falls within  $\mu \pm 2\text{SD}$ . All model equations used in the present study are summarized in Table 2.

## 2.5. Sensitivity analysis

A Monte Carlo sensitivity analysis was conducted to test the sensitivity of simulated spat abundance to environmental factors (i.e. salinity, water temperature, and chl  $a$  concentration) and the variability of demographic parameters (i.e. shape coefficient and half saturation coefficient). The analysis of model sensitivity was performed by varying 2 environmental variables, with the third variable being held constant at 3 levels. We defined 3 levels for each environmental variable as: salinity (low: 10; medium: 20; high: 30), water tem-

perature (low: 10°C; medium: 20°C; high: 30°C), and chl  $a$  concentration (low: 2  $\mu\text{g l}^{-1}$ ; medium: 10  $\mu\text{g l}^{-1}$ ; high: 40  $\mu\text{g l}^{-1}$ ). These values encompass the range experienced by oyster larvae in the GBS. The initial larval abundance was assumed to be 100  $\text{ind. m}^{-2}$  at stages 1–5. The simulation was run 10 000 times in which the values of the first 2 environmental variables were randomly drawn from uniform distributions based on the maximum range potentially encountered by oysters in the GBS. Specifically, salinity (0–40), water temperature (0–40°C), and chl  $a$  concentration (0–40  $\mu\text{g l}^{-1}$ ) were assumed to follow uniform distributions. For each realization, the simulation was run over a 30 d period.

Additionally, we tested the sensitivity of spat abundance to the 2 demographic parameters (i.e. shape coefficient and half saturation coefficient) under favorable environmental conditions (salinity: 20, water temperature: 25°C, and chl  $a$ : 20  $\mu\text{g l}^{-1}$ ). We permuted 1 demographic parameter at various levels (mean + CV, with CV = 0,  $\pm 10\%$ ,  $\pm 20\%$ ,  $\pm 30\%$ ,  $\pm 40\%$ , and  $\pm 50\%$ ), while keeping the other parameter constant at literature values (Table 1). Sensitivity analysis for each parameter at each level of perturbation was conducted 1000 times.

## 2.6. Model validation and simulation

The model simulation for each grid, month, and year began on the day when oyster larvae were sampled and continued for a 30 d period with a daily time step. Larvae are assumed to remain in a given grid for their entire PLD. Daily water temperature, salinity, and chl  $a$  concentration were incorporated to regulate the bioenergetics of each individual in the model. The initial condition in the model was set as stage-specific oyster larval concentration ( $\text{ind. m}^{-3}$ ) observed in our oyster samples. Oyster spawning rate or production rate ( $\text{ind. m}^{-3}$ ) was assumed to be the number of stage-1 larvae (~24–48 h after fertilization) observed in our monthly zooplankton samples. That is, a constant number of new stage-1 recruits was added to the model every day during the simulation. Because bivalve larvae are small and share similar morphology (Garland & Zimmer 2002), approximately 20% of our observed bivalve larvae (H. Liu unpubl. data) were estimated as eastern oyster larvae in our model simulation. We noted that demographic parameters for every individual (e.g. initial size, shape coefficient, half saturation coefficient) varied between realizations, with values randomly drawn from the mean and SD of each parameter.

Table 2. Functional relationships for calculation of model parameters and energy fluxes in the DEBM for eastern oyster larvae

Description	Equation
<b>Physiological rates</b>	
Estimated food density from biomass	$X = 165.23 \times (\text{chl } a)^{1.2504}$
Feeding functional response	$f = \frac{X^2}{X^2 + K^2}$
Maximum volume-specific ingestion rate	$\{\dot{P}_{Xm}\} = C_R \cdot \mu_X$
Ingestion rate	$\dot{P}_X = \{\dot{P}_{Xm}\} \cdot f \cdot V^{2/3} \cdot \alpha_T \cdot \alpha_S$
Assimilation rate	$\dot{P}_A = \kappa_X \cdot \dot{P}_C = \{\dot{P}_{Am}\} \cdot f \cdot V^{2/3} \cdot \alpha_T \cdot \alpha_S$
Reserve mobilization rate	$\dot{P}_C = \frac{\sigma_T \cdot [E] \cdot ([E_G] \cdot \dot{V} \cdot V^{2/3} + [\dot{P}_M])}{\kappa \cdot [E] + [E_G]}$
Energy flux to somatic maintenance	$\dot{P}_{M1} = [\dot{P}_M] \cdot V \cdot \alpha_T$
Energy flux to somatic growth	$\dot{P}_G = \kappa \cdot \dot{P}_C - \dot{P}_{M1}$
Energy flux to development	$\dot{P}_D = (1 - \kappa) \cdot \dot{P}_C - \dot{P}_{M1}$
Energy flux to development maintenance	$\dot{P}_{M2} = [\dot{P}_M] \cdot V \cdot (1 - \kappa) / \kappa \cdot \alpha_T$
<b>Coefficients of environmental forcing</b>	
Temperature correction factor	$\alpha_T = \exp\left\{\frac{T_A - T_1}{T_1} - \frac{T_A}{T}\right\} \cdot \frac{1 + \exp\left\{\frac{T_{AL}}{T_1} - \frac{T_{AL}}{T_L}\right\} + \exp\left\{\frac{T_{AH}}{T_H} - \frac{T_{AH}}{T_L}\right\}}{1 + \exp\left\{\frac{T_{AL}}{T} - \frac{T_{AL}}{T_L}\right\} + \exp\left\{\frac{T_{AH}}{T_H} - \frac{T_{AH}}{T}\right\}}$
Salinity correction factor	$\alpha_S = \begin{cases} 0 & \text{when } S \leq S_L \\ \frac{S - S_L}{S_H - S_L} & \text{when } S \in (S_L, S_H) \\ 1 & \text{when } S \geq S_H \end{cases}$
<b>State variables</b>	
Energy reserve	$\frac{dE}{dt} = \dot{P}_A - \dot{P}_C$
Volume growth rate	$\frac{dV}{dt} = \frac{\dot{P}_G}{[E_G]}$
Length growth rate	$\frac{dL_\omega}{dt} = \left(\frac{\dot{P}_G}{[E_G]}\right) / \frac{1}{3L^2\delta_M}$
Volume shrinkage under starvation	$\frac{dV}{dt} = -\frac{\dot{P}_{M1} - \dot{P}_C}{[E_G]}$
Length shrinkage under starvation	$\frac{dL_\omega}{dt} = \left(\frac{\dot{P}_G}{[E_G]}\right) / \frac{1}{3L^2\delta_M}$
<b>Population model</b>	
Number of individuals at time $t + 1$	$N_{(t+1)} = N_{(t)} - N_{M_s(t)} - N_{M_n(t)}$

Additionally, daily natural mortality in the individual-based modeling framework introduced further stochasticity. To ensure robust results, the simulation was run independently 10 times. The density of spat (ind.  $\text{m}^{-3}$ ) at the end of the 30 d period was collected and converted to the abundance (ind.  $\text{m}^{-2}$ ) on the oyster bed by multiplying the water depth (m).

We defined oyster larval recruitment as the larvae that successfully survived through the pelagic period and settled on the hard substrate as spat. To validate model performance, the observed abundance of newly settled spat (5–25 mm, 1–3 mo old) from

oyster dredge surveys conducted by TPWD was used to compare with our simulated spat abundance. Specifically, we performed a simulation for May 2018 using our larval observations to simulate spat abundance after a 30 d period. We then compared the simulated spat with the average abundance of newly settled spat observed from the TPWD survey in June and July 2018. Details about the TPWD survey methodology are available in Pollack et al. (2012). Our study assumed that the newly settled spat observed by TPWD in June and July predominantly originated from cohorts spawned in May.

Model validation was conducted using the Pearson correlation coefficient ( $r$ ) and the index of agreement (skill) with the formula given below:

$$\text{skill} = 1 - \frac{\sum_{i=1}^n (|y_i - \hat{y}_i|)^2}{\sum_{i=1}^n (|\hat{y}_i - \bar{y}| + |y_i - \bar{y}|)^2} \quad (16)$$

where  $y_i$  is the observation,  $\hat{y}_i$  is the model simulation,  $\bar{y}$  is the overall mean of observations, and  $n$  is the sample size. Note that the skill ranges from 0 (no agreement) to 1 (perfect match). After validation, model simulation was performed, and the results were summarized for the later analysis.

### 2.7. Planktonic habitat suitability

The successful recruitment of oyster larvae largely depends on suitable planktonic habitats that can support optimal reproduction, growth, and survival (Narváez et al. 2012). We summarized the results of observed monthly larval production (ind.  $m^{-2}$ ), cumulative survival rate (%), and growth rate ( $\mu m d^{-1}$ ) to evaluate the planktonic habitat suitability for oyster larvae. These 3 variables ( $VB_i$ ) were normalized from 0 to 1 using the following equation:

$$VB_{i_{\text{normal}}} = \frac{VB_i - VB_i(\text{min})}{VB_i(\text{max}) - VB_i(\text{min})} \quad (17)$$

where  $VB_i(\text{min})$  and  $VB_i(\text{max})$  represent the global minimum and maximum values for variable  $i$ , respectively. Note that values of 1 are optimal, and values of 0 are least suitable. Here, the value of 0 was replaced by 0.001 to avoid zero values.

The normalized variables were combined to calculate planktonic habitat suitability index (PHSI) using a weighted geometric mean function:

$$\text{PHSI} = \left( \prod_{i=1}^n VB_{\text{normal}(i)}^{w(i)} \right)^{1/n} \quad (18)$$

where  $w_{(i)}$  is the weight-normalized variable  $i$ , and  $n$  is the number of variables. We assumed an equal weight ( $w = 1$ ) for each variable, and PHSI was normalized to a range of 0 to 1.

To mitigate potential biased results due to not accounting for larval transport, the biological indices and PHSI of each grid were aggregated into 5 spatial areas that are largely matched with the management areas by TPWD. We assumed a relatively high larval retention rate within each area. In the simulation, we also calculated the demographic traits of oyster larvae such as the PLD and survival rate from stage 1 to stage 6.

### 2.8. Importance of predictor variables

A generalized additive model (GAM; Wood 2003) was developed to examine the effects of predictor variables on oyster larval recruitment. The full GAM was fitted including nonlinear effects of larval production, water temperature, salinity, and chl  $a$  concentration. Backward elimination of predictor variables was used for the model selection, based on Akaike's information criterion (AIC). A model with a minimized AIC value indicates a better model fit. The relative importance of each predictor variable was assessed by comparing the change in AIC ( $\Delta AIC$ ) and the change in percent deviance explained ( $\Delta DE$ , %) between the full model and the reduced model with 1 predictor variable removed. Model development and simulation were performed using MatLab, and statistical analysis was conducted using the RStudio 1.1.463 software.

## 3. RESULTS

### 3.1. Sensitivity analysis

The model output showed strong sensitivity to low levels of salinity (10), water temperature (10°C), and chl  $a$  concentration ( $2 \mu g l^{-1}$ ), with recruitment being significantly lower compared to medium and high levels of these factors (Fig. 3). Moreover, recruitment showed little difference between medium and high levels of salinity, water temperature, and chl  $a$  concentration (Fig. 3). Specifically, recruitment peaked under salinity  $> 10$ , temperatures of 20–30°C, and chl  $a$  concentration  $> 2 \mu g l^{-1}$  (Fig. 3). We found that changes in demographic parameters significantly affected the model output. Specifically, recruitment decreased linearly with the shape coefficient ( $R^2 = 0.82$ , Fig. 4A) and increased linearly with the half saturation coefficient ( $R^2 = 0.93$ , Fig. 4B).

### 3.2. Model validation

Model validation for May 2018 identified recruitment 'hotspots' in the lower Galveston Bay and West Bay (Fig. 5A,B), with simulated spat abundance significantly correlated with observed abundance from TPWD surveys ( $r = 0.72$ ,  $p < 0.0001$ ; Fig. 5C). However, the relationship between simulated and observed values appeared nonlinear, with slight underestimation at low observed values and overestimation at high observed values (Fig. 5C). Despite these deviations, the model simulation demonstrated relatively good agree-

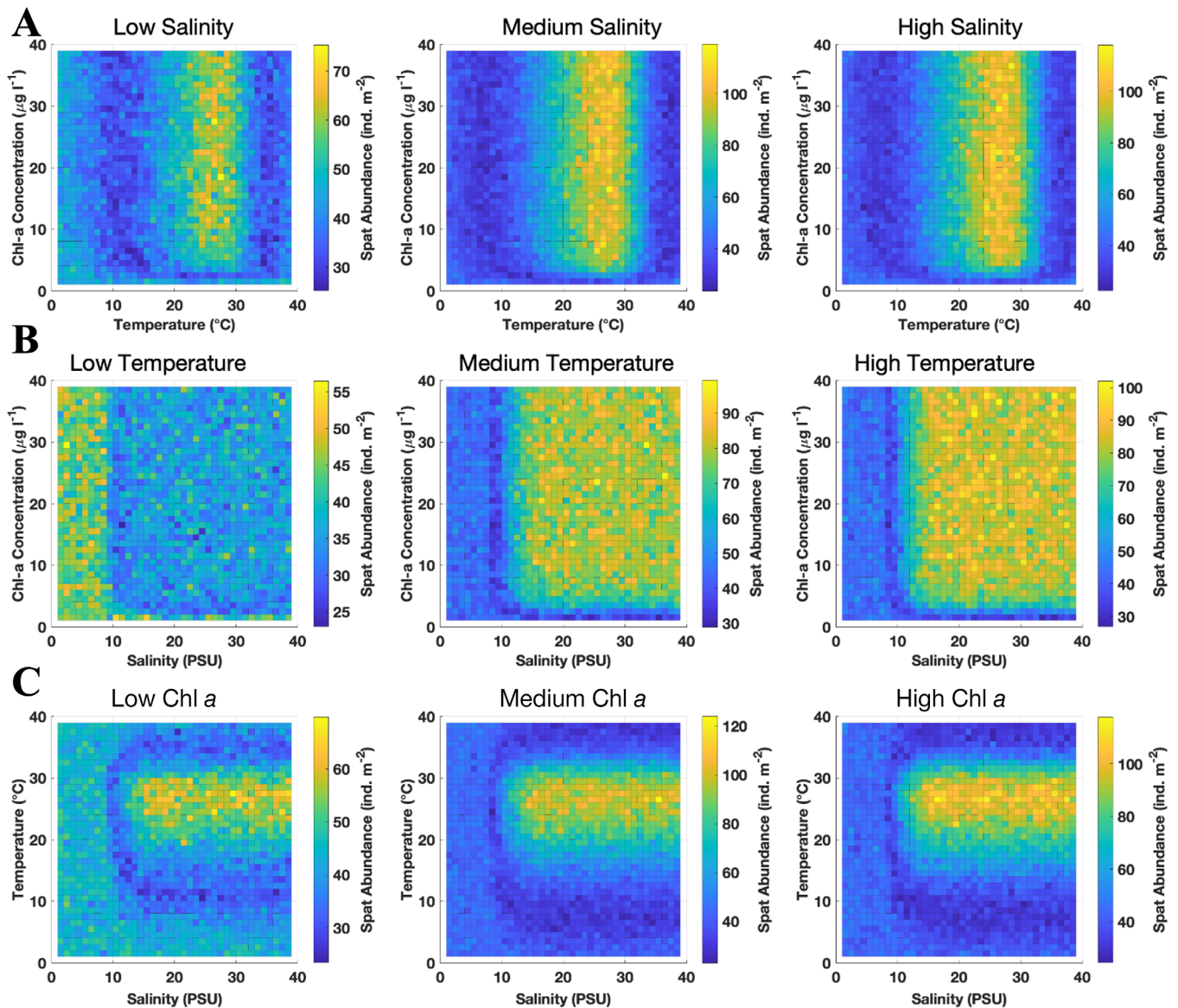


Fig. 3. Sensitivity analysis of environmental factors for oyster spat recruitment (ind. m<sup>-2</sup>). (A) Salinity (low: 10, medium: 20; high: 30); (B) temperature (low: 10°C, medium: 20°C, high: 30°C); (C) chlorophyll *a* (chl *a*) concentration (low: 2 µg l<sup>-1</sup>; medium: 10 µg l<sup>-1</sup>, high: 40 µg l<sup>-1</sup>)

ment with spat observations (skill = 0.82), indicating that the model effectively captured both the spatial patterns and the overall scale of observed abundance.

### 3.3. Larval recruitment

Model simulation depicted the spatio-temporal variations of larval recruitment in the GBS (Fig. 6). In 2018, larval recruitment was elevated in the middle to lower regions of Galveston Bay and throughout most of West Bay, with peak recruitment (up to 25 spat m<sup>-2</sup>) occurring in June (Fig. 6B). This peak was about an order of magnitude higher than the recruitment levels

observed in May and July (Fig. 6A,C). In May 2021, areas of high recruitment (up to 9 spat m<sup>-2</sup>) extended from West Bay to lower Galveston Bay (Fig. 6D,F). After that, high recruitment (up to 18 spat m<sup>-2</sup>) was only maintained in West Bay (Fig. 6E,F).

### 3.4. Larval production, survival, growth, and habitat suitability

Highest larval production (i.e. abundance of new planktonic larvae) was found in upper Galveston Bay in June 2018 and in middle Galveston Bay in July 2021, respectively (Fig. 7A). In addition, very limited

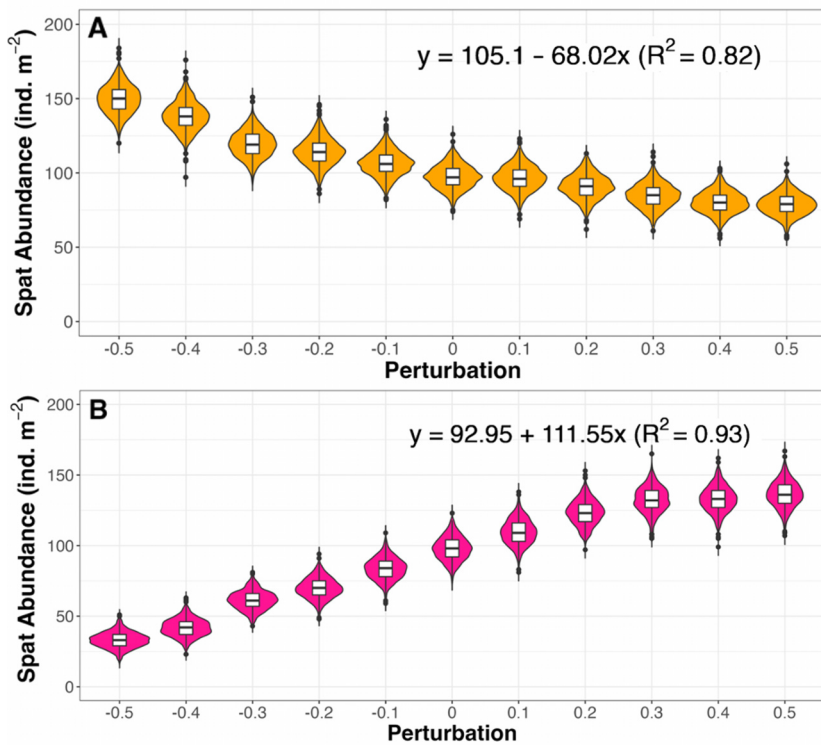


Fig. 4. Sensitivity analysis of spat recruitment ( $\text{ind. m}^{-2}$ ) to demographic parameters of oyster larvae: (A) shape coefficient; (B) half saturation coefficient. Different levels of perturbation were included: mean + CV, with CV = 0,  $\pm 10\%$ ,  $\pm 20\%$ ,  $\pm 30\%$ ,  $\pm 40\%$ , and  $\pm 50\%$ . Boxplots — bar: median; box: interquartile range (IQR); whiskers: max./min. values  $\leq 1.5 \times$  IQR above/below box; dots: outliers

larval production was found in May in both years (Fig. 7A). Oyster survival rates appeared typically high in West Bay and lower Galveston Bay but were sharply reduced in East Bay and in middle–upper Galveston Bay (Fig. 7B). This pattern was consistent across months in both years (Fig. 7B). Optimal growth conditions were observed in West Bay and in middle–upper Galveston Bay, despite temporal variations. Overall, West Bay and lower Galveston Bay appeared to be high-quality habitats, while East Bay (with exceptions in June and July 2018) and upper Galveston Bay (with exceptions in May 2021) generally had lower habitat quality (Fig. 7D). Notably, some areas in middle Galveston Bay could become favorable habitats for oyster recruitment in June 2018 (Fig. 7D).

### 3.5. Demographic traits

PLD calculated from stage 1 to stage 6 (spat stage) ranged from 19.1 to 24.4 d, and no distinct difference was found across months and years (Table 3). The survival rate of planktonic oyster larvae calculated from stage 1 to stage 6 ranged from 1 to 2.7%, with the max-

imum occurring in May 2018 and the minimum occurring in June and July, respectively (Table 3).

### 3.6. Environmental drivers

Results of the GAM indicated that larval production and chl *a* concentration had threshold effects on larval recruitment (Fig. 8A,D). Increasing salinity or temperature within the lower range (5–20 and 25–27°C) positively affected larval recruitment, followed by a negative effect at the upper range (20–30 and 27–31°C) (Fig. 8B,C). Larval recruitment was strongly affected by salinity ( $\Delta\text{AIC} = 626.1$ ,  $\Delta\text{DE} = 32.3\%$ ), followed by larval production ( $\Delta\text{AIC} = 221.5$ ,  $\Delta\text{DE} = 9.3\%$ ), water temperature ( $\Delta\text{AIC} = 97$ ,  $\Delta\text{DE} = 3.9\%$ ), and chl *a* concentration ( $\Delta\text{AIC} = 12.9$ ,  $\Delta\text{DE} = 0.6\%$ ) (Table 4).

## 4. DISCUSSION

In response to hurricane-induced disturbance, the per-capita reproductive potential of remaining oysters may increase due to reduced competition and predation pressure (Livingston et al. 1999). This is supported by our observations of high larval production in the GBS in June 2018, 1 yr after Hurricane Harvey (Fig. 7B). In addition, our findings of high post-hurricane spat recruitment imply that oysters are relatively resilient to the external disturbance. Likewise, a substantial spatfall was reported in Apalachicola Bay, Florida, after Hurricane Elena as a compensating response to massive hurricane-induced oyster die-offs (Livingston et al. 1999). A rapid recovery of oysters was also reported in a south Texas estuary after episodic flood events in 2007 (Pollack et al. 2011). A recent study by Pruet et al. (2021) reported that oyster larvae were tolerant to flood-associated stressors, despite some reduction in oyster growth and survival.

Oyster recovery processes vary at different space–time scales. We found that recovery from successful larval recruitment was likely restricted in middle–upper Galveston Bay and West Bay, where oysters are perennially abundant (Powell et al. 2003). Despite high larval production, recruitment of oyster larvae remained low in upper Galveston Bay, mainly caused

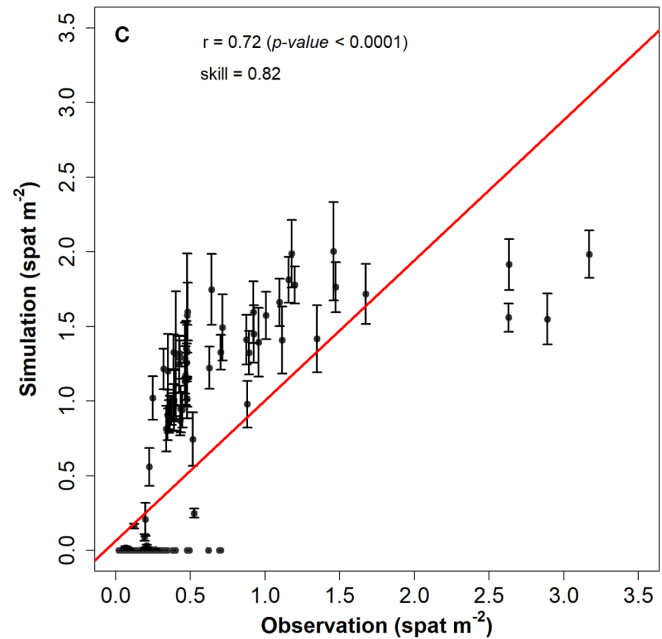
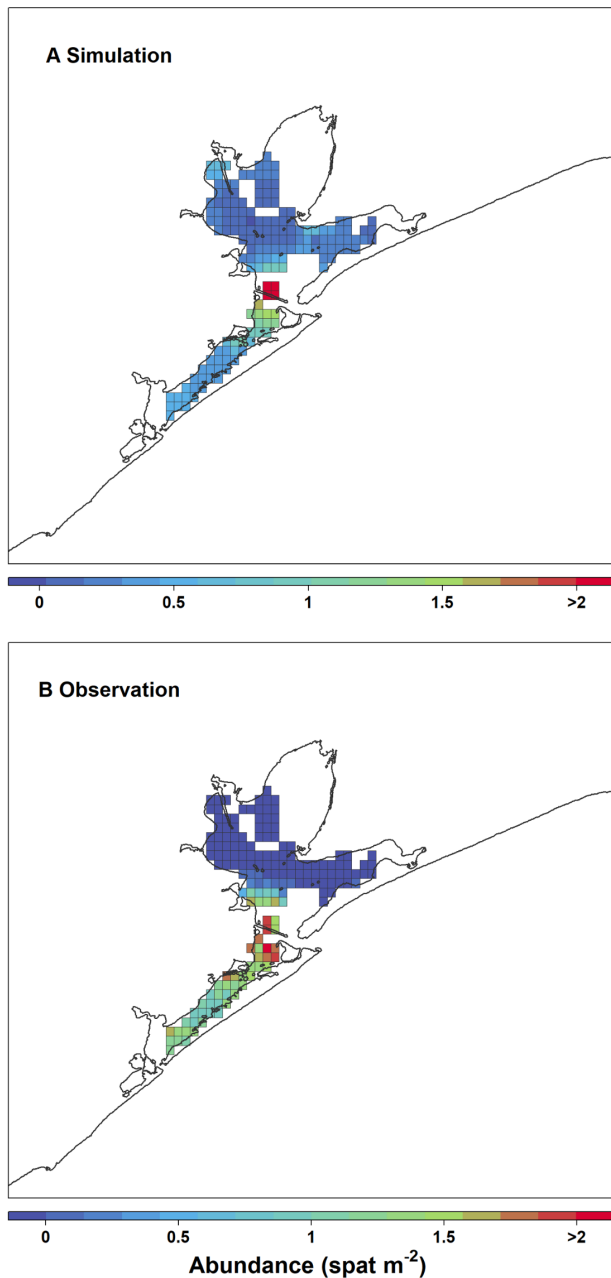


Fig. 5. Spat abundance (spat m<sup>-2</sup>) and distribution in the Galveston Bay System from (A) model simulations and (B) observations. (C) Model validation by the Pearson correlation coefficient ( $r$ ) and the index of agreement (skill). Error bars indicate standard error (SE)

by unfavorable environmental conditions (i.e. low salinity). For example, oyster larvae in this area (near the mouth of the San Jacinto River) may experience frequent freshwater soaking-related physiological stresses, resulting in relatively slow recovery. A previous model simulation of oyster recovery in Delaware Bay after Hurricane Irene and Tropical Storm Lee resulted in a similar finding that oyster populations in the upper bay may take over 10 yr to recover (Munroe et al. 2013). Unlike upper Galveston Bay, recovery in East Bay tends to be inhibited by limited

larval production from our model simulation, which is likely due to post-hurricane mass mortality of spawners (Du et al. 2021). Therefore, a longer recovery period is expected in upper Galveston Bay and East Bay. Successful recruitment in these 2 regions may largely depend on opportunistic colonization during low-flow periods.

Despite low larval survival following Hurricane Harvey, increased larval production, likely driven by density-dependent effects, may help support oyster recovery. This compensating feedback is evident in

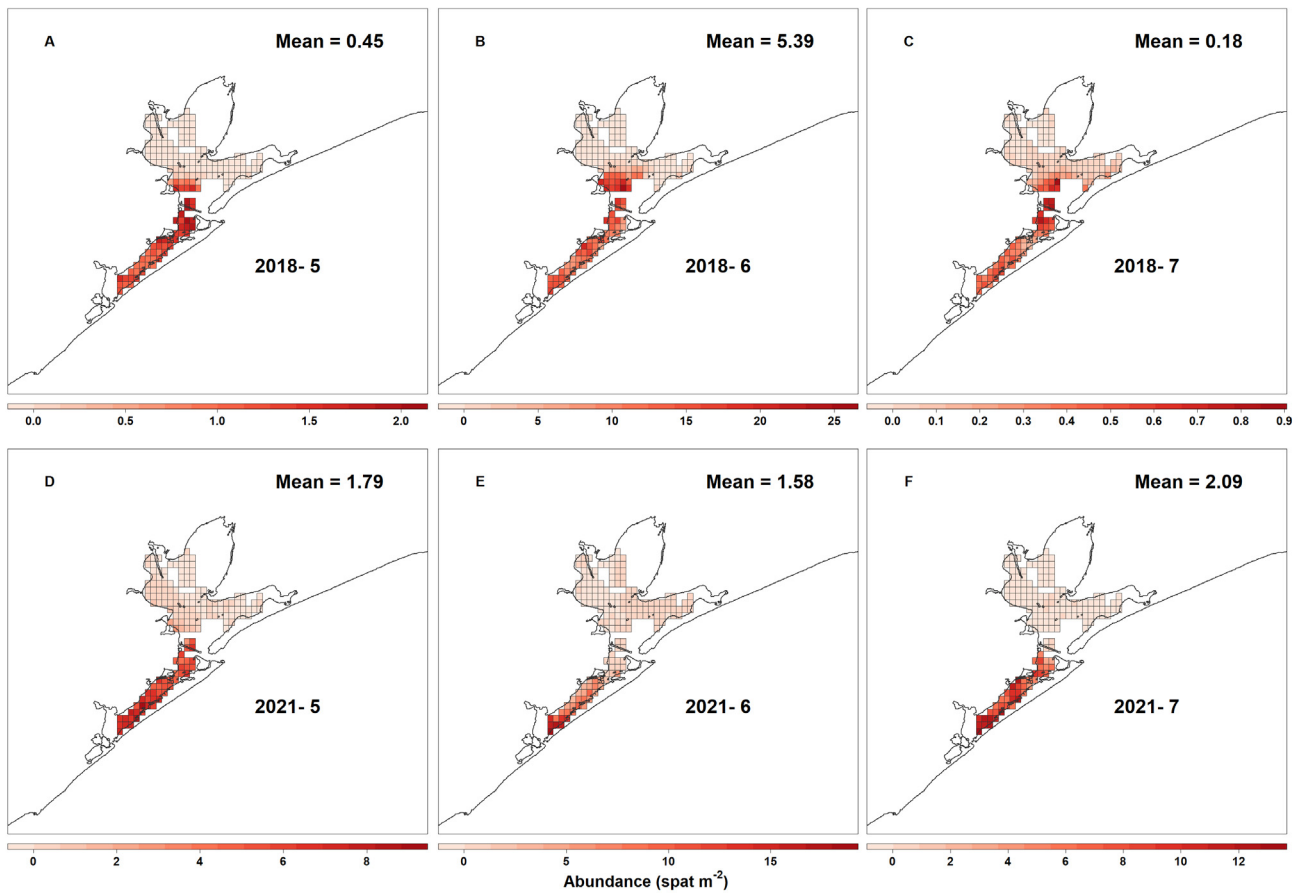


Fig. 6. Simulated oyster larval recruitment ( $\text{spat m}^{-2}$ ) in the Galveston Bay System during the spawning season (May–July: months 5–7) in (A–C) 2018 and (D–F) 2021. The bay-wide mean value is given in each subplot

the sizeable swarm of larvae in June 2018. During normal years, successful recruitment is a result of oyster larval production, survival, and growth. For example, extensive larval recruitment found in May 2021 likely benefits from high rates of survival and growth. A rich larval supply may not guarantee ultimate larval recruitment when survival rate is low. For example, oyster larval recruitment in middle Galveston Bay in June and July 2021 was suppressed by extremely low survival rates, despite the high larval production in this area (Fig. 7). The low survival rate found in June and July 2021 was perhaps caused by prolonged freshwater soaking (Fig. S3). Physiologically, oyster feeding rate decreases as salinity decreases and even ceases when salinity drops below a critical threshold (Casas et al. 2018). Once salinity is low, oyster larvae tend to use reserved energy for somatic maintenance, yet this mechanism may not support oyster survival for a prolonged period due to a tremendous amount of energy deficit (La Peyre et al. 2013).

Planktonic habitat suitability for oyster larvae is synthetically determined by oyster larval production,

survival, and growth. Spatial heterogeneity in planktonic habitat suitability occurred in the GBS (Fig. 7). Lower Galveston Bay and West Bay were categorized as high-quality habitats, and habitat quality degraded toward upper Galveston Bay and East Bay. We note that some areas in upper Galveston Bay and East Bay might become moderately suitable for larval recruitment (Fig. 7) during low freshwater inflow months (Fig. S3). In addition, nutrient levels are relatively high year-round in upper Galveston Bay. Low freshwater discharge, combined with up-stream advected saline water, may lessen low-salinity stress for oyster larvae, which can boost phytoplankton and zooplankton production (Liu et al. 2017, 2021). Hydrodynamics in East Bay and West Bay tend to be relatively stable but driven by different processes (Powell et al. 1995, Rayson et al. 2016). Circulation in East Bay is primarily affected by the inflow from the Trinity River, whereas flow into West Bay can withstand the flooding of freshwater discharge (Powell et al. 1995). Historical records showed that oyster reefs in West Bay were rarely flooded with freshwater (Soniati & Brody

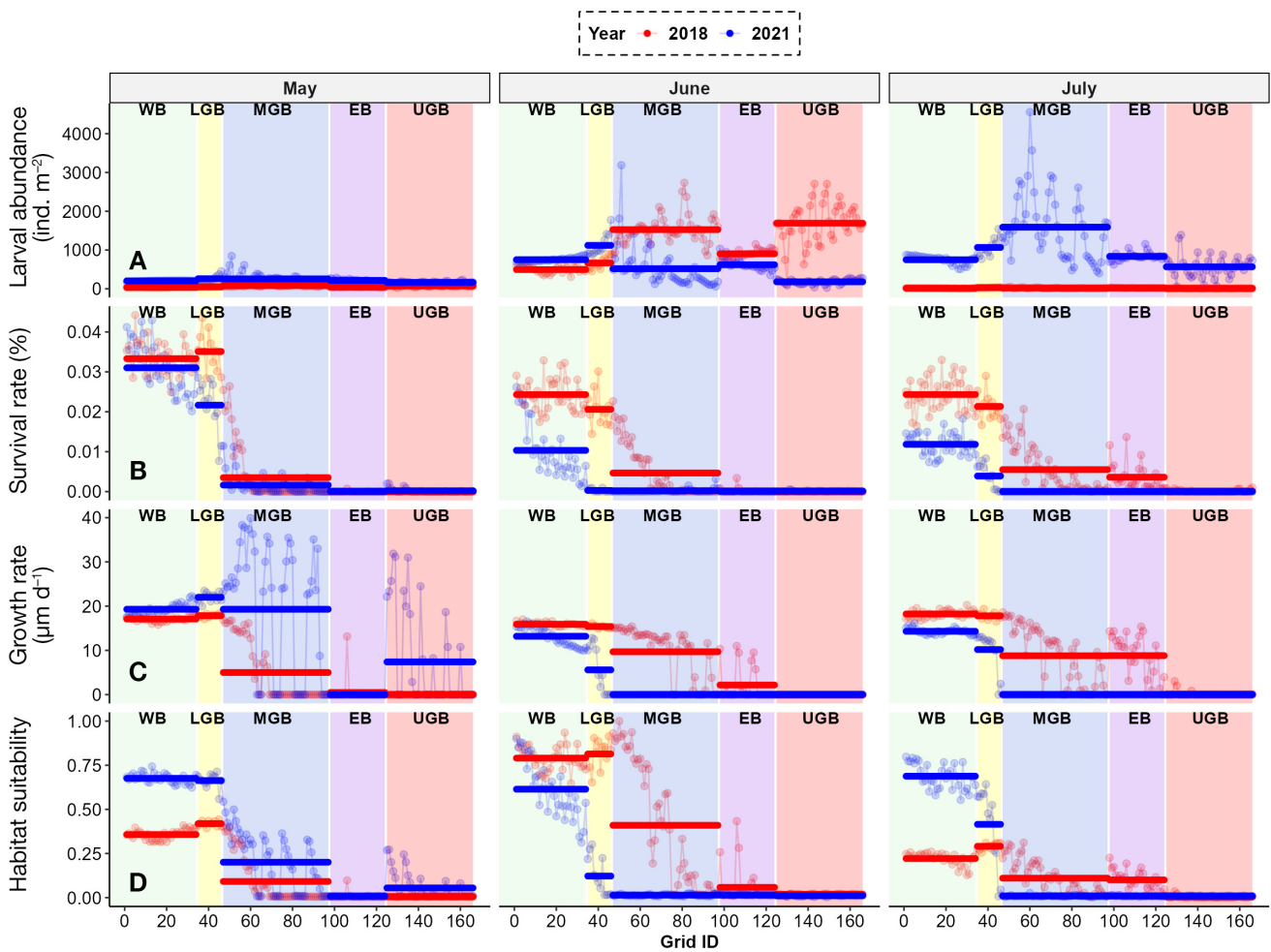


Fig. 7. Results of (A) observed larval abundance, (B) survival rate, (C) growth rate, and (D) planktonic habitat suitability of oyster larvae in the Galveston Bay System during spawning season (May–July) in 2018 and 2021. Blue dots (2018) and red dots (2021) represent the value of each index across different grids (see Fig. 1B for more details). The aggregate mean value of each sub-area (EB: East Bay; LGB: lower Galveston Bay; MGB: middle Galveston Bay; WB: West Bay; UGB: upper Galveston Bay) is also provided (horizontal bars)

1988). However, seasonal pulses of freshwater inflow from the Trinity River (Fig. S3) may disturb the relatively static conditions in East Bay, leading to prolonged unfavorable conditions for planktonic oyster larvae. Hence, the hydrodynamic processes in East Bay and West Bay largely elucidate distinct planktonic habitat quality for oyster larvae even within the similar salinity regime.

Although criteria used to define optimal habitats for settled oysters are well established (Cake 1983, Soniat & Brody 1988, Barnes et al. 2007), limited attention has been paid to planktonic habitat suitability. Here, we attempted to fill the knowledge gap by

Table 3. Mean (SD) planktonic larval duration (PLD) and survival rate of oyster larvae from stage 1 to stage 6 (spat stage) in the Galveston Bay System summarized from model simulation

Demographic trait	2018			2021		
	May	June	July	May	June	July
PLD (d)	21.4 (1.8)	22.6 (2.3)	23.6 (2.7)	19.1 (1.8)	24.4 (3.1)	23.3 (2)
Survival rate (%)	2.7 (1.7)	1.6 (1.2)	1.9 (0.9)	2 (1.6)	1 (1)	1 (0.8)

quantifying planktonic habitat suitability using 3 biologically meaningful indices to exemplify the integrated effects of environmental factors on pelagic habitats. While traditional habitat suitability models for settled oysters typically give equal weights to all candidate variables (Cake 1983, Soniat & Brody 1988)

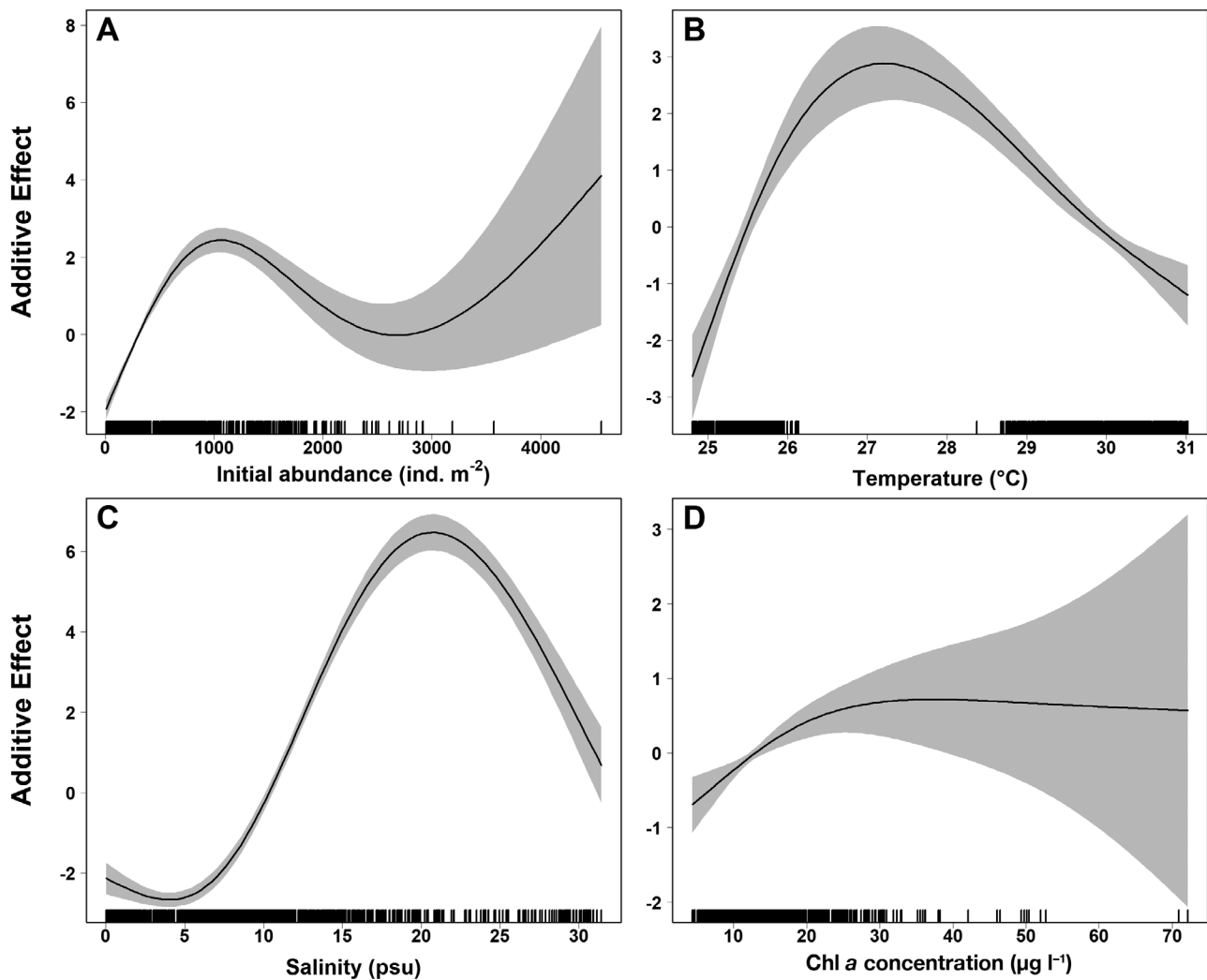


Fig. 8. Response curves for best-fit generalized additive model with 95% confidence bands (shaded areas) for smooth terms of (A) monthly larval production ( $\text{ind. m}^{-2}$ ), (B) temperature ( $^{\circ}\text{C}$ ), (C) salinity, and (D) chlorophyll *a* (chl *a*) concentration ( $\mu\text{g l}^{-1}$ ). The y-axis represents the effect of the predictor

Table 4. Predictor variables retained in the best-fit generalized additive model for oyster larval recruitment (full model baseline values: AIC = 4648.6, DE = 63.3%). Note that a predictor with higher values of changes in Akaike's information criterion ( $\Delta\text{AIC}$ ) and changes in percent deviance explained ( $\Delta\text{DE}$ ) is of higher importance. The effective degrees of freedom (edf) indicate the degree of nonlinearity

Predictor variable	$\Delta\text{AIC}$	$\Delta\text{DE}$ (%)	edf	p
Initial larval abundance	221.5	9.3	3	<0.0001
Water temperature	97	3.9	3	<0.0001
Salinity	626.1	32.3	3	<0.0001
Chl <i>a</i> concentration	12.9	0.6	2.1	<0.0001

in Pollack et al. (2012), a higher weight was given to salinity when calculating habitat suitability for oysters. Our simulation results also highlight the

strong impacts of salinity on oyster recruitment and then on the planktonic habitat suitability.

Statistical analyses further quantified salinity as the primary driver of oyster recruitment. The optimal salinity range found in our study generally agrees with previous observations of maximum reproductive potential at 10–20 (Shumway 1996) and maximum growth at 10–20 (Wang et al. 2008). The effect of temperature was relatively small compared to the significant

impact of salinity in the present study. This is likely attributable to the narrow thermal range (25–31 $^{\circ}\text{C}$ ) of seasonal (May to July) water temperature in

the GBS (Fig. 8). Extremely low (15 and 17.5°C) and high (35°C) water temperatures can cause a drastic reduction in the growth of eastern oyster larvae (Davis & Calabrese 1964), which is echoed in our sensitivity analysis (Fig. 3). In the nGoM estuaries, eastern oysters may experience a wider temperature range over the entire spawning season from April to November (Hopkins 1954); thus, one would anticipate a substantial effect of water temperature on oyster recruitment. In general, bivalve recruitment dynamics may depend not solely on static water temperature per se, but also on the abrupt change in water temperature or thermal shock (Barber & Blake 2006). A previous modeling study suggested that the timing of temperature change is an important factor driving inter-annual variations in oyster reproduction (Hofmann et al. 1992). For example, increased temperature occurring earlier in spring may result in higher reproductive effort (Hofmann et al. 1992). Food concentration acts as a limiting factor for oyster larval growth (Robert et al. 1988). When food conditions are optimal during the spring bloom, chl *a* concentration exerts a lesser impact on larval recruitment. In addition, nutrient loading in the GBS is mainly through seasonal river runoff and is highly variable from year to year (Örnólfsson et al. 2004), which may escalate bottom-up trophic effects that override the temperature effect on oyster larvae.

A few caveats should be noted. First, the boundaries of larval dispersal defined by management areas may affect the accuracy of the predictions. While these boundaries are practical for management purposes, they may not fully capture natural larval dispersal processes. In addition, the utility of the DEBM is not inherently tied to the specific hydrodynamic model used in this study, as we only utilized salinity and temperature simulated from the physical model. The DEBM framework is adaptable and could be integrated with a hydrodynamic model incorporating water circulation in the future to refine predictions of larval dispersal and connectivity. Estuarine water circulation plays a critical role in influencing larval aggregations and settlement patterns (Narváez et al. 2012, Kim et al. 2013). The success of larval settlement is inevitably linked to water circulation processes that transport larvae to suitable habitats with hard substrates. Given the spatial heterogeneity in hydrodynamic processes within the GBS, coupling the current DEBM with a physical circulation model is recommended to better capture the dynamics of oyster larvae in this region. We note that our spat estimates do not perfectly align with observations during model validation, which may be partially attributed to the lack of consideration of post-settlement mortality in

planktonic larvae of marine invertebrates (Lipcius et al. 2007). Post-settlement mortality is not only driven by species bioenergetics but also a variety of biotic and abiotic factors, such as intra- and inter-specific competition. Additionally, spat abundance estimates derived from dredge surveys are subject to bias and spatial variability in dredging efficiency. Dredge efficiency can vary due to gear selectivity, habitat type, and environmental conditions, potentially leading to under- or overestimation of true spat abundance. Further refinements to the model could benefit from incorporating adjustments for dredge efficiency, as highlighted in studies on oyster dredge efficiency (Powell et al. 2007, Marengi et al. 2017) to better link planktonic oyster larvae to oyster recruitment. Salinity data near the deep channel obtained from FVCOM may be underestimated (Fig. S1) due to the complex hydrodynamic conditions. The underestimated salinity could lead to an underestimation of larval recruitment; therefore, estimates of oyster recruitment near the deep channel could be conservative. Given the relatively short PLD of pelagic larvae, high-frequency field sampling is advised for tracking cohort dynamics, prey items, and pelagic habitat conditions. This comprehensive approach combined with continued modeling efforts supports the refinement of the current DEBM. While prolonged low salinity can cause physiological stresses to oysters (Shumway 1996), high salinity tends to indirectly increase oyster mortality by predation and disease (Pollack et al. 2011). In upper Galveston Bay, with high freshwater input, risks of disease and predation may be negligible; however, negative impacts of predation and infection were observed in the moderate–high salinity areas, particularly in West Bay (Soniat & Brody 1988). Last, the model domain in the present study was designed based on existing reef habitats in the GBS, while additional habitats can be generated from dead oyster shells following a significant die-off event, which could aid in oyster recovery after external disturbances (e.g. hurricanes).

Climate-related tropical storms and hurricanes, followed by storm surges and flash flooding, are major disturbances to coastal ecosystems (Patrick et al. 2020, Liu et al. 2021). Ecosystem consequences of large-scale events are often complex because ecological processes often operate at various scales in time and space (Hastings 2010, Li & Liu 2023). Hydrological and biogeochemical variables are sensitive sentinels of hurricane disturbance, and these variables may recover moderately quickly to pre-hurricane levels in days (Patrick et al. 2020) to months (Du & Park 2019). However, post-hurricane pulses of nutrients tend to

boost the pelagic communities through bottom-up regulation, which can cause long-lasting effects on estuarine ecosystems (Liu et al. 2021).

Evidence indicates an increasing prevalence of tropical cyclones in a changing climate (Emanuel 2005). How coastal ecosystems respond to and recover from hurricane disturbance has drawn attention to mitigating the ecological and economic aftermath on ecosystem functioning (Greening et al. 2006). Nevertheless, research on ecosystem-level meaningful responses to hurricanes remains inadequate because it needs to consider the effects from environments to lower and upper trophic levels through an integrated approach with long-term observations and appropriate modeling. Focusing on sensitive ecological indicators to study the ecosystem dynamics is promising (Li & Liu 2023), even though it only provides a snapshot of ecosystem resilience and recovery from natural disasters (Liu et al. 2021). Evaluation of oyster response to hurricanes provides insights into resilience and function of estuarine ecosystems in the face of climate change, which is highly relevant to understanding the adaptation of oyster populations for better management and strategies of the valuable shellfish fisheries to ever-changing climate impacts.

**Acknowledgements.** This study was jointly supported by the National Science Foundation under NSF grant OCE-1760463; Texas Commission on Environmental Quality, Galveston Bay Estuary Program (US-EPA Federal Grant Number: 332023); Texas Parks and Wildlife Department, State Wildlife Grant Program (US-FWS Federal Grant Number: F23AF00081-00); Texas Sea Grant; and TAMUG Comprehensive Research Funds.

#### LITERATURE CITED

- Barber BJ, Blake NJ (2006) Reproductive physiology. *Dev Aquacult Fish Sci* 35:357–416
- Barnes TK, Volety AK, Chartier K, Mazzotti FJ, Pearlstine L (2007) A habitat suitability index model for the eastern oyster (*Crassostrea virginica*), a tool for restoration of the Caloosahatchee Estuary, Florida. *J Shellfish Res* 26: 949–959
- Beck MW, Brumbaugh RD, Airoidi L, Carranza A and others (2011) Oyster reefs at risk and recommendations for conservation, restoration, and management. *BioScience* 61: 107–116
- Bi R, Liu H (2017) Effects of variability among individuals on zooplankton population dynamics under environmental conditions. *Mar Ecol Prog Ser* 564:9–28
- Buck EH (2005) Hurricanes Katrina and Rita: fishing and aquaculture industries — damage and recovery. Report for Congress No. RL34209. Congressional Research Service, The Library of Congress, Washington, DC
- Buzan D, Lee W, Culbertson J, Kuhn N, Robinson L (2009) Positive relationship between freshwater inflow and oyster abundance in Galveston Bay, Texas. *Estuaries Coasts* 32: 206–212
- Cake EW (1983) Habitat suitability index models: Gulf of Mexico American oyster. FWS/OBS 82/10.57. US Department of Interior, Fish and Wildlife Service, Washington, DC
- Casas SM, Lavaud R, La Peyre MK, Comeau LA, Filgueira R, La Peyre JF (2018) Quantifying salinity and season effects on eastern oyster clearance and oxygen consumption rates. *Mar Biol* 165:90
- Coen LD, Brumbaugh RD, Bushek D, Grizzle R and others (2007) Ecosystem services related to oyster restoration. *Mar Ecol Prog Ser* 341:303–307
- Davis HC (1958) Survival and growth of clam and oyster larvae at different salinities. *Biol Bull* 114:296–307
- Davis HC, Calabrese A (1964) Combined effects of temperature and salinity on development of eggs and growth of larvae of *M. mercenaria* and *C. virginica*. *Fish Bull US Fish Wildl Serv* 63:643–655
- Deksheniaks MM, Hofmann EE, Powell EN (1993) Environmental effects on the growth and development of eastern oyster, *Crassostrea virginica* (Gmelin, 1791), larvae: a modeling study. *J Shellfish Res* 12:241–254
- Du J, Park K (2019) Estuarine salinity recovery from an extreme precipitation event: Hurricane Harvey in Galveston Bay. *Sci Total Environ* 670:1049–1059
- Du J, Park K, Jensen C, Dellapenna TM, Zhang WG, Shi Y (2021) Massive oyster kill in Galveston Bay caused by prolonged low-salinity exposure after Hurricane Harvey. *Sci Total Environ* 774:145132
- Emanuel K (2005) Increasing destructiveness of tropical cyclones over the past 30 years. *Nature* 436:686–688
- García-Esquivel Z, Bricelj VM, González-Gómez MA (2001) Physiological basis for energy demands and early post-larval mortality in the Pacific oyster, *Crassostrea gigas*. *J Exp Mar Biol Ecol* 263:77–103
- Garland ED, Zimmer CA (2002) Techniques for the identification of bivalve larvae. *Mar Ecol Prog Ser* 225: 299–310
- Galtsoff PS (1964) The American oyster, *Crassostrea virginica* Gmelin. *Fish Bull US Fish Wildl Serv* 64:1–480
- Grabowski JH, Brumbaugh RD, Conrad RF, Keeler AG and others (2012) Economic valuation of ecosystem services provided by oyster reefs. *BioScience* 62:900–909
- Greening H, Doering P, Corbett C (2006) Hurricane impacts on coastal ecosystems. *Estuaries Coasts* 29:877–879
- Guthrie CG, Matsumoto J, Solis RS (2012) Analysis of the influence of water plan strategies on inflows and salinity in Galveston Bay. Final report to the United States Army Corps of Engineers. Contract No. R100010015. Texas Water Development Board, Austin, TX
- Hanley TC, Hughes AR, Williams B, Garland H, Kimbro DL (2016) Effects of intraspecific diversity on survivorship, growth, and recruitment of the eastern oyster across sites. *Ecology* 97:1518–1529
- Hastings A (2010) Timescales, dynamics, and ecological understanding. *Ecology* 91:3471–3480
- Haws MC, DiMichele L, Hand SC (1993) Biochemical changes and mortality during metamorphosis of the Eastern oyster, *Crassostrea virginica*, and the Pacific oyster, *Crassostrea gigas*. *Mol Mar Biol Biotechnol* 2:207
- Hofmann EE, Powell EN, Klinck JM, Wilson EA (1992) Modeling oyster populations. 3. Critical feeding periods, growth and reproduction. *J Shellfish Res* 11:399–416

- Holling CS (1959) Some characteristics of simple types of predation and parasitism. *Can Entomol* 91:385–398
- Hopkins AE (1935) Oysters in Galveston Bay, Texas. *Bull Bur Fish* 47:57–83
- Hopkins SH (1954) Oyster setting on the Gulf coast. *Proc Natl Shellfish Assoc* 45:52–55
- Jackson JBC (2001) What was natural in the coastal oceans? *Proc Natl Acad Sci USA* 98:5411–5418
- Jager T, Ravagnan E (2015) Parameterising a generic model for the dynamic energy budget of Antarctic krill *Euphausia superba*. *Mar Ecol Prog Ser* 519:115–128
- Jones G, Jones B (1983) Methods for setting hatchery produced oyster larvae. Information report no. 4. Marine Resources Branch, Ministry of Environment, Victoria, BC
- Kennedy VS (1996) Biology of larvae and spat. In: Kennedy VS, Newell RIE, Eble AF (eds) *The eastern oyster: Crassostrea virginica*. Maryland Sea Grant Publications, College Park, MD, p 371–421
- Kim C, Park K, Powers SP (2013) Establishing restoration strategy of eastern oyster via a coupled biophysical transport model. *Restor Ecol* 21:353–362
- Klein JC, Powell EN, Kreeger DA, Ashton-Alcox KA and others (2023) Modeling performance and settlement windows of larval eastern oyster (*Crassostrea virginica*) in Delaware Bay. *J Shellfish Res* 42:437–463
- Kooijman SALM (2000) *Dynamic energy and mass budgets in biological systems*. Cambridge University Press, Cambridge
- La Peyre MK, Eberline BS, Soniat TM, La Peyre JF (2013) Differences in extreme low salinity timing and duration differentially affect eastern oyster (*Crassostrea virginica*) size class growth and mortality in Breton Sound, LA. *Estuar Coast Shelf Sci* 135:146–157
- Lavaud R, La Peyre MK, Casas SM, Bacher C, La Peyre JF (2017) Integrating the effects of salinity on the physiology of the eastern oyster, *Crassostrea virginica*, in the northern Gulf of Mexico through a Dynamic Energy Budget model. *Ecol Model* 363:221–233
- Li C, Liu H (2022) Exploring cosmopolitan jellyfish (*Aurelia* spp.) bloom dynamics and ecological implications in subtropical waters with mechanistic dynamic modeling. *J Mar Syst* 228:103705
- Li C, Liu H (2023) Comparative ecosystem modelling of dynamics and stability of subtropical estuaries under external perturbations in the Gulf of Mexico. *ICES J Mar Sci* 80:1303–1318
- Lipcius RN, Eggleston DB, Heck KL Jr, Seitz RD, Van Montrans J (2007) Post-settlement abundance, survival, and growth of post larvae and young juvenile blue crabs in nursery habitats. In: Kennedy VS, Cronin LE (eds) *The blue crab Callinectes sapidus*. Maryland Sea Grant, College Park, MD, p 535–564
- Liu H, Zhang X, Yang Q, Zuo T, Quigg A (2017) Mesozooplankton dynamics in relation to environmental factors and juvenile fish in a subtropical estuary of the Gulf of Mexico. *J Coast Res* 33:1038–1050
- Liu H, Gilmartin J, Li C, Li K (2021) Detection of time-varying pulsed event effects on estuarine pelagic communities with ecological indicators after catastrophic hurricanes. *Ecol Indic* 123:107327
- Livingston RJ, Howell IV, Robert L, Niu X, Lewis GF III, Woodsum GC (1999) Recovery of oyster reefs (*Crassostrea virginica*) in a Gulf estuary following disturbance by two hurricanes. *Bull Mar Sci* 64:465–483
- Marenghi F, Ashton-Alcox K, Wong R, Reynolds B, Ozbay G (2017) Dredge efficiency on natural oyster grounds in Delaware Bay and its application in monitoring the Eastern oyster (*Crassostrea virginica*) stock in Delaware, USA. *Fish Res* 186:292–300
- Martinez MJ, Palmer TA, Breaux NJ, Pollack JB (2022) Dynamics of restored and natural oyster reefs after a hurricane. *Front Ecol Evol* 10:791739
- Monaco CJ, Wetthey DS, Helmuth B (2014) A dynamic energy budget (DEB) model for the keystone predator *Pisaster ochraceus*. *PLOS ONE* 9:e104658
- Munroe D, Tabatabai A, Burt I, Bushek D, Powell EN, Wilkin J (2013) Oyster mortality in Delaware Bay: impacts and recovery from Hurricane Irene and Tropical Storm Lee. *Estuar Coast Shelf Sci* 135:209–219
- Narváez DA, Klinck JM, Powell EN, Hofmann EE, Wilkin J, Haidvogel DB (2012) Modeling the dispersal of eastern oyster (*Crassostrea virginica*) larvae in Delaware Bay. *J Mar Res* 70:381–409
- North EW, Schlag Z, Hood RR, Li M, Zhong L, Gross T, Kennedy VS (2008) Vertical swimming behavior influences the dispersal of simulated oyster larvae in a coupled particle-tracking and hydrodynamic model of Chesapeake Bay. *Mar Ecol Prog Ser* 359:99–115
- Orlando SP Jr, Rozas LP, Ward GH, Klein CJ (1993) Salinity characteristics of Gulf of Mexico estuaries. National Oceanic and Atmospheric Administration, Office of Ocean Resources Conservation and Assessment, Silver Spring, MD
- Örnólfsson EB, Lumsden SE, Pinckney JL (2004) Nutrient pulsing as a regulator of phytoplankton abundance and community composition in Galveston Bay, Texas. *J Exp Mar Biol Ecol* 303:197–220
- Park K, Powers SP, Bosarge GS, Jung H (2014) Plugging the leak: Barrier island restoration following Hurricane Katrina enhances larval retention and improves salinity regime for oysters in Mobile Bay, Alabama. *Mar Environ Res* 94:48–55
- Patrick CJ, Yeager L, Armitage AR, Carvallo F and others (2020) A system level analysis of coastal ecosystem responses to hurricane impacts. *Estuaries Coasts* 43: 943–959
- Pollack JB, Kim H, Morgan EK, Montagna PA (2011) Role of flood disturbance in natural oyster (*Crassostrea virginica*) population maintenance in an estuary in South Texas, USA. *Estuaries Coasts* 34:187–197
- Pollack JB, Cleveland A, Palmer TA, Reisinger AS, Montagna PA (2012) A restoration suitability index model for the Eastern oyster (*Crassostrea virginica*) in the Mission-Aransas Estuary, TX, USA. *PLOS ONE* 7:e40839
- Pouvreau S, Bourles Y, Lefebvre S, Gangnery A, Alunno-Bruscia M (2006) Application of a dynamic energy budget model to the Pacific oyster, *Crassostrea gigas*, reared under various environmental conditions. *J Sea Res* 56:156–167
- Powell EN, Klinck JM, Hofmann EE, Wilson-Ormond EA, Ellis MS (1995) Modeling oyster populations. V. Declining phytoplankton stocks and the population dynamics of American oyster (*Crassostrea virginica*) populations. *Fish Res* 24:199–222
- Powell EN, Klinck JM, Hofmann EE, McManus MA (2003) Influence of water allocation and freshwater inflow on oyster production: a hydrodynamic–oyster population model for Galveston Bay, Texas, USA. *Environ Manag* 31: 0100–0121
- Powell EN, Ashton-Alcox KA, Kraeuter JN (2007) Reevalua-

- ation of eastern oyster dredge efficiency in survey mode: application in stock assessment. *N Am J Fish Manag* 27: 492–511
- ✦ Pruettt JL, Pandelides AF, Willett KL, Gochfeld DJ (2021) Effects of flood-associated stressors on growth and survival of early life stage oysters (*Crassostrea virginica*). *J Exp Mar Biol Ecol* 544:151615
- ✦ Quayle DB (1964) Distribution of introduced marine Mollusca in British Columbia waters. *J Fish Res Board Can* 21:1155–1181
- ✦ Rayson MD, Gross ES, Hetland RD, Fringer OB (2016) Time scales in Galveston Bay: an unsteady estuary. *J Geophys Res Oceans* 121:2268–2285
- ✦ Rico-Villa B, Bernard I, Robert R, Pouvreau S (2010) A Dynamic Energy Budget (DEB) growth model for Pacific oyster larvae, *Crassostrea gigas*. *Aquaculture* 305:84–94
- ✦ Robert R, His E, Dinét A (1988) Combined effects of temperature and salinity on fed and starved larvae of the European flat oyster *Ostrea edulis*. *Mar Biol* 97:95–100
- ✦ Roelke DL, Li HP, Hayden NJ, Miller CJ, Davis SE, Quigg A, Buyukates Y (2013) Co-occurring and opposing freshwater inflow effects on phytoplankton biomass, productivity and community composition of Galveston Bay, USA. *Mar Ecol Prog Ser* 477:61–76
- ✦ Schaeffer BA, Kurtz JC, Hein MK (2012) Phytoplankton community composition in nearshore coastal waters of Louisiana. *Mar Pollut Bull* 64:1705–1712
- Shumway S (1996) Natural environmental factors. In: Kennedy VS, Newell RIE, Eble AF (eds) *The eastern oyster: Crassostrea virginica*. Maryland Sea Grant Publications, College Park, MD, p 467–513
- ✦ Smee DL, Overath RD, Johnson KD, Sanchez JA (2013) Intra-specific variation influences natural settlement of eastern oysters. *Oecologia* 173:947–953
- ✦ Soniat TM, Brody MS (1988) Field validation of a habitat suitability index model for the American oyster. *Estuaries* 11:87–95
- ✦ Soniat TM, Conzelmann CP, Byrd JD, Roszell DP, Bridevaux JL, Suir KJ, Colley SB (2013) Predicting the effects of proposed Mississippi River diversions on oyster habitat quality; application of an oyster habitat suitability index model. *J Shellfish Res* 32:629–638
- ✦ Sprung M (1984) Physiological energetics of mussel larvae (*Mytilus edulis*). III. Respiration. *Mar Ecol Prog Ser* 18: 171–178
- Tunnell JW Jr (2017) Shellfish of the Gulf of Mexico. In: Ward CH (ed) *Habitats and biota of the Gulf of Mexico: before the Deepwater Horizon oil spill*. Vol 1: Water quality, sediments, sediment contaminants, oil and gas seeps, coastal habitats, offshore plankton and benthos, and shellfish. Springer, New York, NY, p 769–839
- ✦ van der Veer HW, Cardoso JF, van der Meer J (2006) The estimation of DEB parameters for various Northeast Atlantic bivalve species. *J Sea Res* 56:107–124
- ✦ Wang H, Huang W, Harwell MA, Edmiston L and others (2008) Modeling oyster growth rate by coupling oyster population and hydrodynamic models for Apalachicola Bay, Florida, USA. *Ecol Model* 211:77–89
- ✦ Wood SN (2003) Thin plate regression splines. *J R Stat Soc Ser B Stat Methodol* 65:95–114
- ✦ Yang Z, Richardson P, Chen Y, Kelley JGW and others (2016) Model development and hindcast simulations of NOAA's Gulf of Maine operational forecast system. *J Mar Sci Eng* 4:77

Editorial responsibility: Romuald Lipcius,  
Gloucester Point, Virginia, USA

Reviewed by: 4 anonymous referees

Submitted: December 21, 2023; Accepted: January 16, 2025

Proofs received from author(s): March 8, 2025

This article is Open Access under the Creative Commons by Attribution (CC-BY) 4.0 License, <https://creativecommons.org/licenses/by/4.0/deed.en>. Use, distribution and reproduction are unrestricted provided the authors and original publication are credited, and indicate if changes were made